Computer simulation of the structure and elasticity of polyurethane networks: 1. Polyoxypropylene tetrols and hexamethylene diisocyanate

K.-J. Lee and B. E. Eichinger*
Department of Chemistry, BG-10, University of Washington, Seattle, WA 98195, USA
(Received 24 March 1989; revised 23 June 1989; accepted 8 July 1989)

Model urethane networks prepared from polyoxypropylene tetrols and hexamethylene diisocyanate have been studied with the aid of the computer. Good agreement with experiment is found for gel points when the crosslinkers are treated as sticks. The simulation-theory moduli for the phantom model show good agreement with experiments for networks prepared with $M_n = 1200$ in the bulk and at various dilutions, or with $M_n = 2100$ in the bulk. Simulations underestimate moduli for networks prepared from $M_n = 2100$ at various dilutions by factors of less than 2.

(Keywords: urethane; networks; polyoxypropylene; elasticity)

INTRODUCTION

Random network structures are very complex, and no known experimental techniques can directly investigate these structures in any detail. Although theories[1–4] have focused on these problems, no detailed account of the all-important cycles in random networks has yet been given. Theories of cyclization[5,6] and measurements of the extent of cyclization[7] have been given, but these results have not elucidated the myriad of structures that are produced during network formation. Off-lattice computer simulations, as developed by Leung and Eichinger[8], offer an alternative method to investigate in detail quantities such as the extent of cyclization, cycle rank, dangling ends and sol–gel distributions. The algorithm has been adapted to simulate critical gel points[9], mechanical properties[10,11], the end-linking of polyol stars with bifunctional groups[12] and the radiation cure of polymers[13,14].

The algorithm used to simulate the end-linking of triol stars with bifunctional groups[12] is used here to investigate the structures and physical properties of urethane networks. The Gaussian chains that were used in previous studies[12] are here replaced by ones generated by a Monte Carlo method[15–20] based on the rotational isomeric state (RIS) theory[21]. Techniques to generate Monte Carlo polymer chains have been developed in our previous work[11].

Model networks prepared from polyols and diisocyanates have been extensively studied by Ilavský and Dušek[22–24] and by Stepto and coworkers[25–28]. The focus of this paper is on the systems that were studied experimentally by Stepto[27,28]. In one series of studies, tetrols (*Figure 1*), which were synthesized by reacting pentaerythritol with propylene oxide, were polymerized with hexamethylene diisocyanate (HDI)[29]. The polymerizations were carried out at 80°C in the bulk and at various dilutions in nitrobenzene. Our purpose here is to compare the results of computer simulations with those of the measurements[29], which include gel points α_c and reduced moduli $\tilde{G}$. The experimental data that are addressed in these simulations were kindly provided by Professor R. F. T. Stepto[29]. These data were not shown in refs. 27 and 28.

STATISTICAL WEIGHT MATRICES FOR POP TETROLS

The conformation energies of polyoxypropylene (POP) were first investigated by Abe *et al.*[30]. Their results provide parameters used here to generate chain configurations of POP tetrols with a Monte Carlo–RIS scheme. A segment of an isotactic POP chain is shown in its planar, all-*trans* configuration in *Figure 2*. The bond lengths l_{C-O} and l_{C-C} are 0.143 and 0.153 nm, respectively[30]. Supplements of the bond angles[30] O–C–C and C–O–C are 70°. All asymmetric carbon atoms have the *R* configuration for simplicity. The three different statistical weight matrices needed for the repeating bonds C–C,

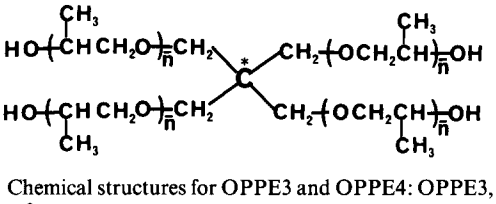

Figure 1 Chemical structures for OPPE3 and OPPE4: OPPE3, $\bar{n} \simeq 5$; OPPE4, $\bar{n} \simeq 9$

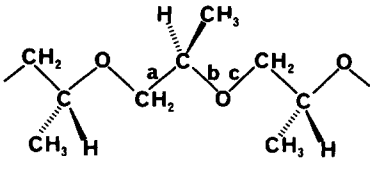

Figure 2 A segment of the isotactic poly((*R*)-oxypropylene) chain in its planar all-*trans* configuration

* To whom correspondence should be addressed

0032-3861/90/030406-08

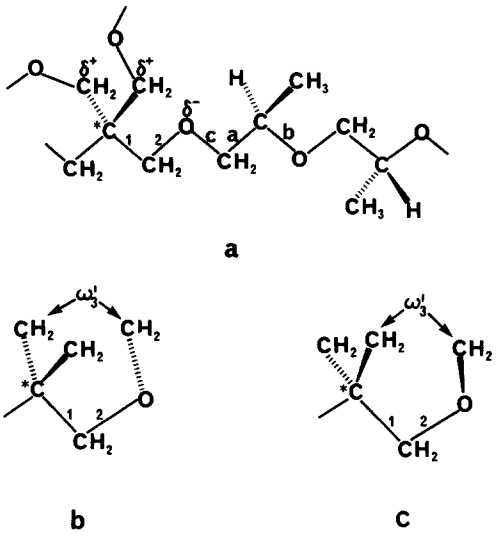

Figure 3 Stereo configuration focused on bonds 1 and 2 for one arm of a tetrol molecule. (a) *Trans* conformation at bond 1; δ^+ and δ^- denote partial positive and negative charges, respectively. (b) The *gauche*-plus (g^+) about bond 2. (c) The *gauche*-minus (g^-) about bond 2

C–O and O–C in *Figure 2* are U_a^R, U_b^R and U_c^R, respectively. These matrices are given by[30]:

$$U_a^R = \begin{bmatrix} 1 & \alpha & \beta \\ 0 & \alpha & \beta\omega \\ 1 & \alpha\omega & 0 \end{bmatrix} \quad (1a)$$

$$U_b^R = \begin{bmatrix} 1 & 0 & 1 \\ 1 & 0 & \omega \\ 1 & 0 & 1 \end{bmatrix} \quad (1b)$$

$$U_c^R = \begin{bmatrix} 1 & \sigma & 0 \\ 1 & 0 & 0 \\ 1 & 0 & \sigma \end{bmatrix} \quad (1c)$$

where superscripts R denote the stereochemical configuration at the asymmetric tertiary carbon atoms, and rows and columns are indexed in the order t, g^+ and g^- for the state of the preceding bond and for the state of the bond in question, respectively. Here statistical weight parameters α, β and σ are defined for the first-order interactions and ω for the second-order interactions, and their corresponding energies[30] used in the present calculations are $E_\alpha = -0.3$, $E_\beta = 0.5$, $E_\sigma = 0.9$ and $E_\omega = 0.4\,\text{kcal mol}^{-1}$. The corresponding matrices for a unit having the S configuration at the tertiary carbon may be easily derived from those of the R unit by the equation[21]:

$$U^S = QU^RQ \quad (2)$$

where

$$Q = \begin{bmatrix} 1 & 0 & 0 \\ 0 & 0 & 1 \\ 0 & 1 & 0 \end{bmatrix} \quad (3)$$

The statistical weight matrices of equations (1) are applied to the repeating units indicated by the parentheses in *Figure 1*. The remaining bonds, which are not repeating, may be safely taken to be *trans*. *Figure 3a* depicts a portion of a tetrol in the neighbourhood of the nexus. There are partial charges[31] $\delta_C = 0.155$ and $\delta_O = -0.31$ that generate an interaction energy[31] between CH_2 and O of $-0.4\,\text{kcal mol}^{-1}$ belonging to the first-order interaction σ_3 in POM_3 (polyoxytrimethylene) chains[31]. Therefore, there is a very high probability that bond 1 is in the *trans* state. The *gauche*-plus (g^+) and *gauche*-minus (g^-) states for bond 2 are shown in *Figures 3b* and *3c* when bond 1 is kept in the *trans* state. The interaction $CH_2 \cdots CH_2$ has a very high energy, so that the statistical weight parameter[31] $\omega_3' = 0$. Saiz *et al.*[32] have shown that the two C–O bonds of poly(3,3-dimethyl oxetane) (PDO) are restricted to the *trans* state. Hence, bond 2 is most likely to be found in the *trans* state.

SIMULATION PROCEDURE

The algorithm that had been used previously for simulations with polyol stars[12] required appropriate modifications to address the systems studied by Stepto[29]. New code, parametrized as described above, was used to generate POP tetrol configurations by Monte Carlo–RIS methods. In the simulations, the central carbon atoms of the POP tetrols, *C in *Figure 1*, and diisocyanates were randomly distributed in a cubical box whose edge length was determined by the total volume of gel, sol and solvent in the system at the end of network formation. More specifically, the reactive ends of the polyols were positioned in the box as follows. The arms were first generated out from the central carbon atom (*C) by use of the RIS scheme. Details of the procedure have been given by Hill and Stepto[15], by Yoon and Flory[16] and by DeBolt and Mark[20]. After having generated four arms, the whole molecule was positioned at random in the box with an overall orientation determined by a random unit vector generator[33]. The number of molecules that were generated was fixed by the size of the simulation.

The conditions for bond formation between –OH (A) and –NCO (B) are the same as those given in previous studies[8]. Briefly, the algorithm functions as follows. Each isocyanate group is visited in turn and distances between each and the unreacted hydroxyl ends are determined. Distances that fall within a prescribed capture sphere are saved and tabulated. The capture sphere represents, in an average sense, the volume throughout which molecules may diffuse in a unit of time (we do not attempt to establish a relationship between reaction time and extent of reaction in this work). The table of pair distances is then sorted from the smallest to the largest and bond formation proceeds in that order. Details of the connections that are formed are recorded during the bond formation process. One difference between this and previous work is that, once a urethane linkage (A–B) formed, the diisocyanate was moved. The crosslinkers were treated as sticks of length L in these movements; in previous studies[12], the diisocyanates were treated as points. This was done because the POP tetrols modelled in this work have low molecular weights, and the size of the diisocyanate is not negligible by comparison with the length of one arm of a tetrol. The movement of HDI units was controlled by the following conditions: (a) there is only one unreacted functional group on the crosslinker; (b) the unreacted NCO group was placed a distance L from the end of the arm with which the diisocyanate reacted; and (c) the orientation of the HDI was determined by a random unit vector generator[33]. During the linkage process, the program keeps track of the details of connectivity for all molecules and analyses them with

a spanning tree program (SPANFO)[34], which sorts the gel from the sol components. Structures such as two-arm loops, double-edge loops and various types of dangling ends are then enumerated. For a given configuration of chains, the capture radius is increased step by step to span a range of extents of reaction, and molecular connectivities are recorded for each step.

The overall density of network chains and crosslinkers is controlled by input parameters that duplicate the physical densities that were used in the experiments. The overall distribution of molecules is random, but of course the ends of polymer chains are correlated with one another. We do not attempt to model the detailed space fillings of the backbones of the molecules in these simulations. Details of the chain packing are unimportant for simulations on networks of this type because the reactive groups are relatively dilute. If we were to include a very difficult computation of the radial distribution of molecular centres it would likely entail the motions of reactive groups by only a few ångströms and that would not perturb the topological structures that are generated by the linking algorithm. (Clearly there are situations, such as the sulphur cure of polyisoprene, where the local liquid-like structure of the molecules will play an important role in determining the statistics of bond formation and, in particular, the probability for formation of small loops. That level of detail is simply not required for the systems under investigation.) It might be further mentioned that, apart from the movement of the diisocyanates to the chain ends in order to get the probabilities for loop formation correct, we do not undertake movements of larger molecules. The reason for omitting movements is that we have previously engaged in extensive explorations of the consequences of these motions and have found that they are inconsequential in terms of the structures of the networks that are produced.

When the distance between unreacted A and B groups in the gel becomes large, it is likely that they will not be able to approach one another owing to the constraints imposed by the connectivity of the gel. At high conversion, the restrictions on the diffusion of network junctions due to the neighbouring chains may be very severe. Flory[35] has shown that the mean-square fluctuations of junctions $\langle \Delta r^2 \rangle$, in the absence of constraints (Gaussian phantom network), is:

$$\langle \Delta r^2 \rangle = (2/f)\langle r^2 \rangle_0 \quad (4)$$

where $f=4$ in this work and $\langle r^2 \rangle_0$ is the mean-square end-to-end distance between two –OH groups of a tetrol. In this work, when the capture radius increased to $2\langle r^2 \rangle_0^{1/2}$, the gel–gel reactions were suppressed, but gel–sol reactions were allowed. The choice of the arbitrary length $2\langle r^2 \rangle_0^{1/2}$ is based loosely on equation (4), and on the observation that, when the capture radius is equal to $2\langle r^2 \rangle_0^{1/2}$, the probability of cyclization is very low. Therefore, it is reasonable to suppress gel–gel reactions when the capture radius is greater than $2\langle r^2 \rangle_0^{1/2}$. The advantage of this procedure is that the capture radius can then be increased to almost equal the length of the reaction box, thereby allowing sol molecules to find one another or unreacted sites on the gel, and thus allowing nearly complete reaction. At high conversions, only one large particle is observed and is identified as the gel. The small species that remain are the sol.

Calculations were done on systems of 10000 tetrol molecules with isotactic chains. (Results for distribution functions of isotactic and atactic chains will be shown later.) The number of crosslinkers N_c used was determined by:

$$N_c = 4r_s N_p / f_b \quad (5)$$

where $r_s = [\text{NCO}]/[\text{OH}] = 1.0$ is the stoichiometric ratio, N_p is the number of the tetrol molecules and $f_b = 2$ is the functionality of the crosslinker. The length L between two NCO groups of hexamethylene diisocyanate (HDI) was taken to be 1.26 nm. This value of L was determined from $\langle r^2 \rangle_0^{1/2}$ for six methylene (CH_2) groups[21] and two isocyanate (NCO) groups, the value of $\langle r^2 \rangle_0^{1/2}$ being obtained by Monte Carlo–RIS methods for an alkane with seven skeletal bonds. Simulations were performed on two different molecular weights of POP tetrols (OPPE3 and OPPE4)[27,28] in the bulk and at various dilutions at 80°C, having arms with degrees of polymerization 5 and 9, respectively.

The number-average molecular weights are 1200 g mol^{-1} (OPPE3) and 2100 g mol^{-1} (OPPE4). The number-average functionalities f_n are 3.96–3.99[29]. For some systems, crosslinkers were treated both as sticks and as points. Unless otherwise specified, the results given were obtained by treating the crosslinkers as sticks. The densities[29] of networks and solvent used in these calculations are 1.02, 1.05 and 1.145 g cm^{-3} for OPPE3, OPPE4 and nitrobenzene, respectively. The values of $2\langle r^2 \rangle_0^{1/2}$ are 2.55 nm for OPPE3 and 4.35 nm for OPPE4. The method used to calculate $\langle r^2 \rangle_0$ for OPPE3 and OPPE4 will be given later. All results obtained are averages over at least four configurations for each set of parameters. Edge effects are imperceptible, as in previous studies[8,9], if more than about 5000 tetrol molecules are generated.

RESULTS AND DISCUSSION

Distribution functions and $\langle r^2 \rangle_0$

The end-to-end distance r between two –OH groups on the same tetrol molecule with isotactic and atactic POP chains was calculated according to Monte Carlo–RIS methods. The end-to-end distances r were normalized by nl, and these values were grouped into 20 equally spaced intervals. Plots of the proportion of scaled end-to-end distances occurring in each interval as a function of r/nl directly give the non-Gaussian distribution $W(r)$. Results at 80°C obtained for the tetrol molecules with isotactic chains having 34 (OPPE3) and 58 (OPPE4) skeletal bonds are shown in *Figure 4* as full curves. Results for atactic chains are plotted as dotted curves. It is clear that the distribution functions for isotactic chains are essentially the same as those for atactic chains, which justifies the simplification of taking all chains to be isotactic. (We do not know the tacticity of the molecules used in the experiments.) *Figure 4* also shows Gaussian distributions (broken curves), which were calculated from:

$$nlW(r) = (3/2\pi\langle \rho^2 \rangle_0)^{3/2} 4\pi\rho^2 \exp(-3\rho^2/2\langle \rho^2 \rangle_0) \quad (6)$$

where $\rho = r/nl$ and $\langle \rho^2 \rangle_0 = C_n/n$. The characteristic ratios[36] C_n used here are 4.24 for $n=34$ and 4.52 for $n=58$. As can be seen from *Figure 4*, the departures of the RIS distributions from the Gaussian are much greater than those for POE (polyoxyethylene)[11]. This could be due to differences in characteristic ratios or to differences

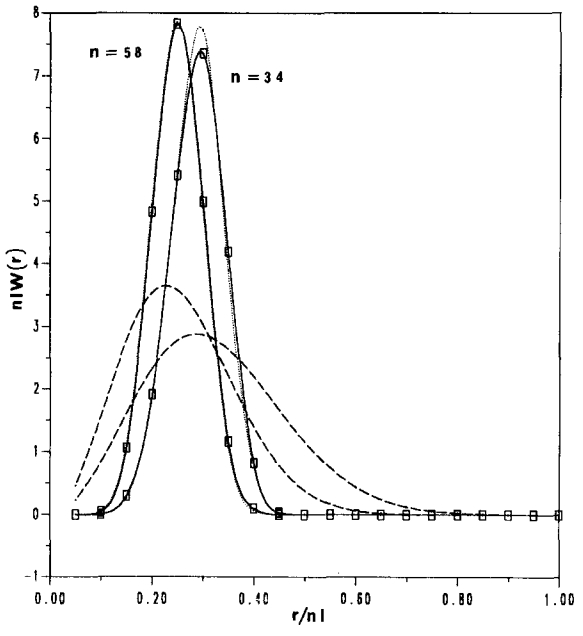

Figure 4 End-to-end distance distribution functions obtained from the Monte Carlo–RIS scheme for POP tetrols having $n=34$ and 58 at 80°C: isotactic chains (full curves), atactic chains (dotted curves). Gaussian distributions for $n=34$ and 58 are also shown (broken curves)

Table 1 The dominant sol constituents

x-mer	Graph	$10^2 w_x$[a]	$10^2 w_x$[b]	$10^2 w_x$[c]	$10^2 w_x$[d]
1	✕	0.01	0.01	0.06	0.07
	✕○	0.03	0.02	0.04	0.08
		0.58	0.61	0.33	0.52
2	○○	0.00	0.01	0.01	0.01
Others	○✕○	0.03	0.04	0.03	0.13

[a] $M_n=1200$, 0.0 wt% solvent, $p=0.964$ and $w_s=0.65\%$
[b] $M_n=1200$, 14.9 wt% solvent, $p=0.962$ and $w_s=0.69\%$
[c] $M_n=2100$, 0.0 wt%solvent, $p=0.963$ and $w_s=0.47\%$
[d] $M_n=2100$, 20.4 wt% solvent, $p=0.961$ and $w_s=0.81\%$

in geometry. POP chains are stiffer than POE because of the methyl groups[37].

The mean-squared end-to-end distances $\langle r^2\rangle_0$ in the unperturbed state were calculated according to the equation:

$$\langle r^2\rangle_0=\sum_i r_i^2 p_i \qquad (7)$$

where r_i and p_i are the end-to-end distances and the probability in each interval, respectively.

The sol portion

The compositions of several major constituents of the sol are tabulated in *Table 1*. Results were obtained by reacting two different molecular weights ($M_n=1200$ and $M_n=2100$) of tetrol monomers with HDI to extents of reaction of ~96%. *Table 1* lists only the first two systems of these two different molecular weights (weight per cent of solvent equal to 0.0 and 14.9 for OPPE3 and 0.0 and 20.4 for OPPE4), which had very low sol fractions. Results for other systems are omitted for brevity. *Table 1* shows that there are two major types of molecules in the sol. They are tetrol monomers and cyclic molecules that contain two-arm loops, double-loop monomers (butterfly) and dumbbells. It can be seen that the most abundant molecules are double-loop monomers, which constitute ~89% of the weight of the sol for $M_n=1200$ and ~69% for $M_n=2100$.

The gel point

General methods to estimate the gel points by use of computer simulations have been investigated by Shy *et al.*[9]. Results obtained by the upper–lower bound method to estimate the gel points have given very good agreement between simulations[12] and measurements[7]. The maximum reduced average cluster size[38] (RDP_w) has been used to locate the lower bound[9], and the inflection point in plots of the weight-average degree of polymerization (DP_w) vs. the extent of reaction (p) has been used to estimate the upper bound[9]. Whenever there are two or more large particles, RDP_w reaches a maximum value, which gives a lower bound to the true gel point. When these particles are incorporated into a single large particle, there is a rapid increase in the slope in the DP_w distribution. Newton's interpolation method[39] was used to estimate the maximum slope, which is an upper bound. *Figure 5* shows examples for two systems of plots of DP_w and RDP_w vs. the extents of reaction (p).

Gel points[1] are characterized by $\alpha_c=(p_A p_B)_c$, the critical value of the product of the extents of reaction of A and B groups at gelation. The tree-like model[1] of branching theory gives $\alpha_c=1/(f-1)$. Since this gelation theory neglects cycles formed before the gel point, it underestimates the true gel point. The average of the upper and lower bounds gives the critical point of p_A or p_B ($r_s=1$) at gelation. The results for α_c obtained by simulations are entered in column 4 of *Table 2*. It can be seen that the agreement between simulations and experiments[29] (column 3 of *Table 2*) is quite good when the crosslinkers are treated as sticks.

The ring-forming parameter λ_{AB} introduced by Ahmad and Stepto[40] can be determined from α_c by means of the equation:

$$\alpha_c(f-1)(1-\lambda_{AB})^2=1 \qquad (8)$$

where λ_{AB} gives the competition between inter- and

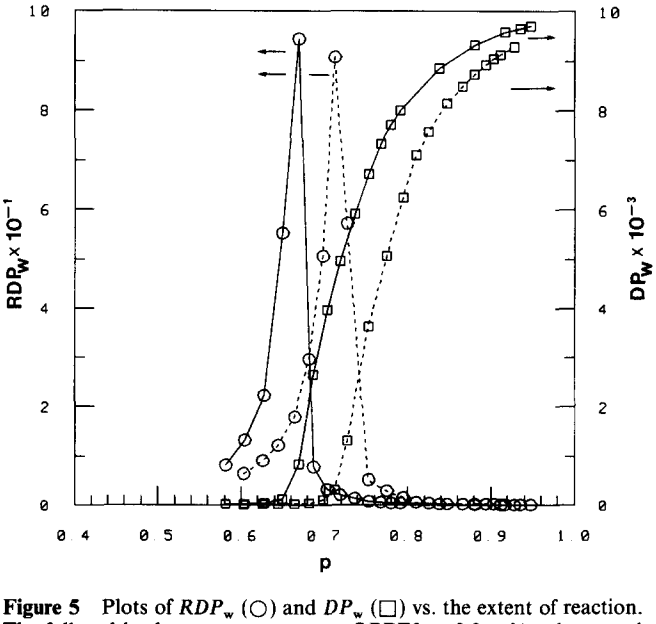

Figure 5 Plots of RDP_w (○) and DP_w (□) vs. the extent of reaction. The full and broken curves represent OPPE3 at 0.0 wt% solvent and OPPE4 at 59.9 wt% solvent, respectively

Table 2 Gel points and fraction of loops[a]

M_n	Conc.[b]	α_c[c]	α_c[d]	λ_{AB}[e]	f_l[f]
1200 (OPPE3)	0.00	0.445	0.456 (0.552)	0.134	0.095 (0.143)
	14.9	0.462	0.462 (0.592)	0.151	0.098 (0.166)
	30.0	0.492	0.480 (0.626)	0.177	0.117 (0.189)
	48.9	0.515	0.522	0.195	0.146
	69.9	0.545	0.577	0.218	0.199
2100 (OPPE4)	0.00	0.445	0.432 (0.511)	0.134	0.071 (0.093)
	20.4	0.471	0.446 (0.522)	0.159	0.086 (0.113)
	39.7	0.502	0.498 (0.550)	0.185	0.113 (0.130)
	50.0	0.512	0.507	0.193	0.128
	59.9	0.535	0.528	0.211	0.149

[a] Values obtained by treating crosslinkers as points are given in parentheses
[b] Reaction concentration, wt% solvent
[c] Experimental concentration, wt% solvent
[d] This work
[e] Ring-forming parameter calculated from equation (8)
[f] This work, fraction of loops at gel point

intramolecular reaction, i.e.:

$$\lambda_{AB}=\frac{c_{int}}{c_{int}+c_{ext}} \tag{9}$$

Here c_{int} is the local concentration of the reactive groups on the same molecule, and c_{ext} is the local concentration of reactive groups on other molecules. Values entered in column 5 of *Table 2* are calculated according to equation (8) by using $f=4$ and the experimental values of α_c in column 3 of *Table 2*. Data in the last column of *Table 2* are the number of loops per total (inter- and intramolecular) reaction at the gelation points from the simulations. It can be seen that the values of λ_{AB} are always higher than the fraction of chains forming loops from the simulations. Also, the values of λ_{AB} are insensitive to different molecular weights. For lower molecular weight and high dilutions, the simulation values approach the calculated values of λ_{AB}. When the crosslinkers are treated as points the agreement between λ_{AB} and the values in parentheses of the last column for OPPE3 are reasonably good. Data in columns 4 and 6 show that there is more loop formation and the gel points increase by as much as 5–14% when the crosslinkers are treated as points.

As the molecular weight varies from 2100 to 1200, the critical value α_c obtained in the bulk shifts from 0.432 to 0.456 (see column 4 of *Table 2*) because of the greater extent of loop formation for lower molecular weight (see column 6 of *Table 2*). For the same molecular weight, α_c increases as the reaction system becomes more dilute. This results from the greater probability for loop formation with increasing dilution. These results for cyclization are similar to those of previous studies[9,11].

The gel portion

To aid comparisons, data in the first three columns of *Table 3* are the same as those of the experiments[29]. Values in column 4 of *Table 3* are the weight fractions of the sol w_s obtained by adjusting the capture radii to the extents of reaction shown in column 5 of *Table 3*. Values for the experimental sol fractions (column 3 of *Table 3*) are lower than those of simulations for systems of lower molecular weight and for that in the bulk of higher molecular weight. The simulations generate many double-loop molecules, which cause the sol fractions to be large. Assuming that these simulations are an accurate rendering of the experimental system, we conclude that real sol molecules are trapped in the gel to a considerable extent.

Under the experimental conditions[7,41], side-reactions to form allophanate groups are probable, and this may have lowered the sol fractions in the experimental systems. The numbers of active groups relative to the number of polyol arms incorporated into the gel are entered in the last column of *Table 3*. An active group is either an –NCO group or active –OH in the gel. According to the simulation results, there exists ~4% of free NCO groups when the extent of reaction is ~96%.

The structures of the gel

The dominant structural irregularities that exist in the topology of these networks are three-arm dangling ends (dangling ends with three free arms) and two-arm loop defects. Three-arm dangling ends are formed by attachment of only one arm of a tetrol monomer to the network. Two-arm loops are formed when the two active arms of a tetrol monomer connect to the same crosslinker. The algorithm can identify five types of three-arm dangling ends and two types of two-arm loops. The symbols for these fragments are shown in *Figures 6, 8,* and *10*. The population η of each irregularity is expressed in terms of the number of fragments per tetrol monomer incorporated into the gel.

The systems that were simulated have been shown in *Table 2*. For brevity, only some of these systems are presented in the figures. *Figures 6* and *7* show how the various populations η of the three types of three-arm dangling ends depend on the extent of reaction (p). The symbols for these three types of dangling ends connected to saturated junctions (degree = 4) are designated as 'I', 'V' and 'ψ'. The dots on the symbols represent the central

Table 3 Extent of reaction and weight fraction of sol[a]

M_n	Conc.[b]	w_s[c]	w_s[d]	p[e]	a_c[f]
1200 (OPPE3)	0.00	0.27	0.65 (2.02)	0.964 (0.962)	0.073 (0.074)
	14.9	0.35	0.69 (2.13)	0.962 (0.958)	0.077 (0.095)
	30.0	0.49	1.05 (2.85)	0.958 (0.962)	0.084 (0.077)
	48.9	1.34	1.40	0.958	0.088
	69.9	2.25	2.95	0.951	0.110
2100 (OPPE4)	0.00	0.33	0.47 (0.80)	0.963 (0.963)	0.068 (0.068)
	20.4	0.82	0.81 (1.15)	0.961 (0.964)	0.071 (0.067)
	39.7	1.11	1.10 (1.41)	0.957 (0.963)	0.077 (0.076)
	50.0	3.97	3.85	0.914	0.083
	59.9	5.10	5.05	0.903	0.086

[a] Values obtained by treating crosslinkers as points are given in parentheses
[b] Reaction concentration, wt% solvent
[c] Sol fraction, ref. 29
[d] Sol fraction, this work
[e] Extent of reaction, this work
[f] Number fraction of active groups in the gel, this work

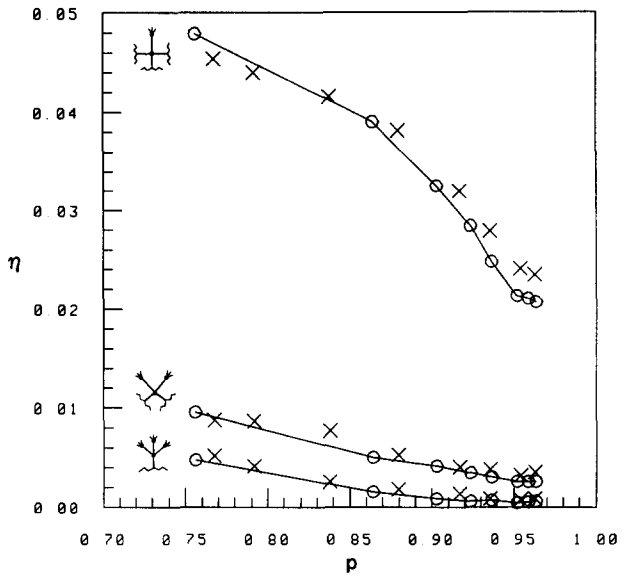

Figure 6 Plots of (from top) populations of 'I', 'V' and 'ψ' dangling ends vs. the extent of reaction for different molecular weights in the bulk: OPPE3 (×) and OPPE4 (○)

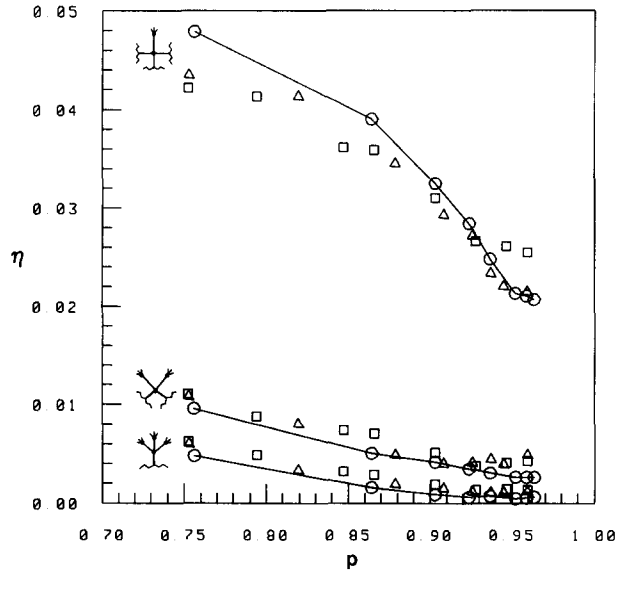

Figure 7 Plots of (from top) populations of 'I', 'V' and 'ψ' dangling ends vs. the extent of reaction for OPPE4 in solutions: bulk (○), 39.7% (△) and 59.9% (□)

carbon atoms (*C) of the POP tetrol molecules (*Figure 1*). The remainder of the network is denoted by jagged lines. *Figures 6* and *7* also show that the populations of the three types of dangling ends are independent of the molecular weight (*Figure 6*) and dilution (*Figure 7*). It is clear from the figures that the populations of types V and ψ approach zero at high conversion. This is because types V and ψ are converted into type I, as network formation proceeds, and type I disappears by connecting to unsaturated cyclic molecules in the sol or to another part of the network.

The symbols for dangling ends connected to unsaturated tetrol monomers (degree = 3) are designated as 'I_3' and 'V_3'. *Figures 8* and *9* show the various populations for I_3 and V_3 as functions of the extent of reaction. The populations of I_3 and V_3 approach zero at high conversion since the monomers to which I_3 and V_3 are attached become saturated or types I_3 and V_3 connect to another part of the network. Once again, *Figures 8* and *9* show that types I_3 and V_3 are insensitive to molecular weight (*Figure 8*) and reaction concentrations (*Figure 9*).

There are two types of loop defects: two-arm inner loops, whose junctions are saturated; and two-arm dangling loops, the junctions of which are unsaturated. The various populations of these loops defects vs. the extent of reaction are shown in *Figures 10* and *11*. As reactions proceed, the dangling loops can be converted to inner loops. Therefore, the curves for dangling loops (the lower parts of *Figures 10* and *11*) fall quickly, and those for inner loops (the upper parts of *Figures 10* and *11*) increase dramatically. As in previous studies[9,11], the populations of loop defects depend on both molecular weight and dilution. *Figure 10* shows that the lower-molecular-weight tetrol gives more loop formation in the

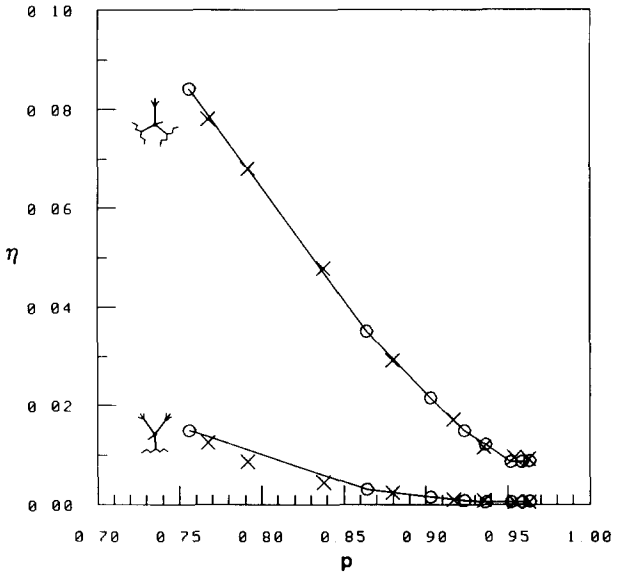

Figure 8 Plots of (from top) populations of 'I_3' and 'V_3' dangling ends vs. the extent of reaction for OPPE3 and OPPE4 in the bulk: symbols are the same as those of *Figure 6*

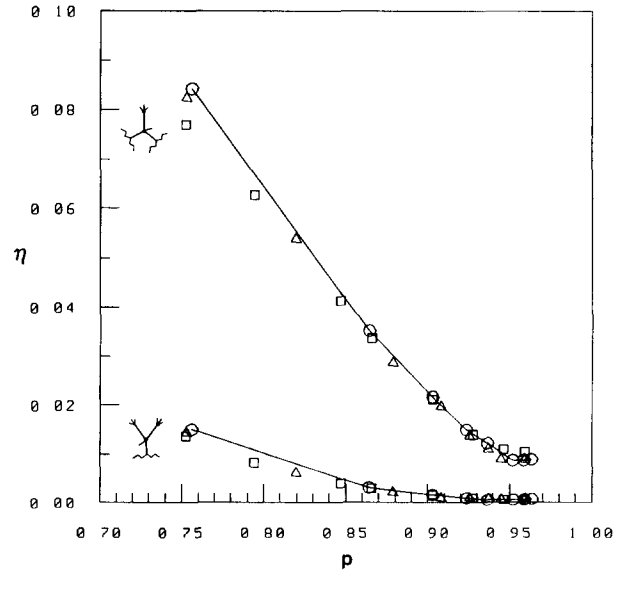

Figure 9 Plots of (from top) populations of 'I_3' and 'V_3' dangling ends vs. the extent of reaction for OPPE4 in solutions: symbols are the same as those of *Figure 7*

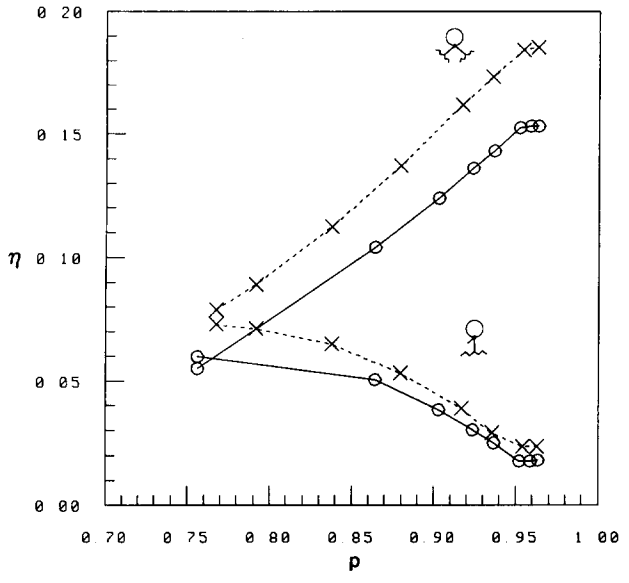

Figure 10 Population of dangling loops (lower curves) and inner loops (upper curves) for OPPE3 and OPPE4 in the bulk: symbols are the same as those of *Figure 6*

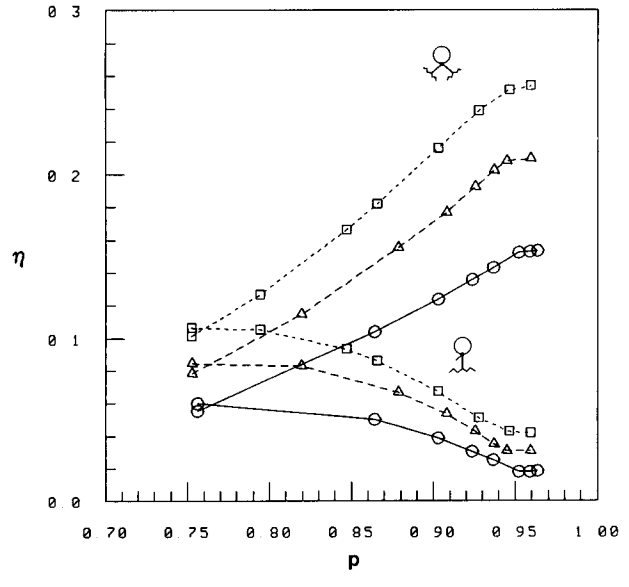

Figure 11 Population of dangling loops (lower curves) and inner loops (upper curves) for OPPE4 in solutions: symbols are the same as those of *Figure 7*

bulk, and *Figure 11* shows that cyclization is enhanced by increasing dilution for OPPE4.

The elasticity modulus

The shear modulus G derived from the elementary Gaussian theory is given by[25,42]:

$$G = ART\rho v_2^{1/3}(V_{gel}/V_f)^{2/3}/M_c \qquad (10)$$

where v_2 is the volume fraction of the swollen network at the time of measurement, V_{gel} is the volume of the dry, unstrained network, and V_f is the volume of the network at formation. The density of the dry network is ρ, M_c is the effective molar mass between elastically active junction points, and A has the value $(1-2/f)$ for phantom networks and the value 1 for affine networks. For perfect tetrafunctional networks, $M_c/AM_c^0 = 1$ for affine behaviour and $M_c/AM_c^0 = 2$ for phantom behaviour. Here, M_c^0 is the molar mass between elastically active junctions.

Data in column 5 of *Table 4* give the reduced moduli $\tilde{G}^0$ (ref. 29). These values were obtained by reducing equation (10) to a reference state at 300 K, $A = 1$ and $\rho = 1$. The reduced modulus is:

$$\tilde{G}^0 = 300R/M_c \qquad (11)$$

Moduli obtained from the simulations according to the phantom network model are entered in the last column of *Table 4*. The entries in this column were calculated from:

$$\tilde{G}^0 = (\xi_a/V_0)300R \qquad (12)$$

where ξ_0 is the cycle rank, and V_0 is the volume of the dry network with density $\rho = 1$. (Note that, in order to facilitate comparisons, V_0 is calculated with $\rho = 1$ instead of the actual density of the networks.)

In these simulations, cycle ranks are calculated from:

$$\xi_a = \nu_a - \mu_a \qquad (13)$$

where ν_a and μ_a are the number of active chains and active junctions[43,44], respectively. An active junction is one that is connected by at least three paths to the network, and an active chain is terminated by active junctions at both ends. According to these definitions, an active junction is a vertex (original tetrol monomer) in the molecular graph whose degree is greater than 2, and an active chain (two arms from different monomers and one crosslinker) is attached to two different active junctions. If a three-arm dangling end or a two-arm dangling loop is attached to a junction (vertex) whose degree is equal to 4, the network wastes one active chain. If a junction's degree is equal to 3 (unsaturated tetrol monomer), only two arms of which connect to the network, for example type I_3 in *Figure 8*, it is excluded from the count of active junctions. Although the degree of an inner loop's junction is equal to 4, it is excluded from the count of active junctions. Using this counting scheme, active chains and active junctions can be readily

Table 4 Reduced modulus[a]

M_n	Conc.[b]	w_s[c]	p[d]	$10^{-5}\tilde{G}^{0}$[e]	$10^{-5}\tilde{G}^{0}$[f]
1200	0.00	0.65	0.964	10.5±1.9	9.776
(OPPE3)		(2.02)	(0.962)		(8.078)
	14.9	0.69	0.962	10.9±2.9	9.440
		(2.13)	(0.958)		(7.286)
	30.0	1.05	0.958	11.1±2.3	8.642
		(2.85)	(0.962)		(7.019)
	48.9	1.40	0.958	10.1±1.5	7.773
	69.9	2.95	0.951	8.5±1.7	5.673
2100	0.00	0.47	0.963	8.1±1.7	6.836
(OPPE4)		(0.80)	(0.963)		(6.304)
	20.4	0.81	0.961	9.5±1.2	6.449
		(1.15)	(0.964)		(5.941)
	39.7	1.10	0.957	7.7±1.3	5.866
		(1.41)	(0.963)		(5.371)
	50.0	3.85	0.914	7.2±0.6	4.684
	59.9	5.05	0.903	7.7±1.3	4.019

[a] Values obtained by treating crosslinkers as points are given in parentheses
[b] Reaction concentration, wt% solvent
[c] Sol fractions (simulation)
[d] Extent of reaction (simulation)
[e] Reduced modulus in $N\,m^{-2}$ (measurement)
[f] Reduced modulus in $N\,m^{-2}$ (simulation)

obtained from the results of the simulations. The results of this scheme for calculating cycle ranks are the same as those for effective chains ν and effective junctions μ[8,11], since Graessley[45] and Flory[46] have proved that $\nu - \mu = \nu_a - \mu_a$.

From the values in columns 5 and 6 in *Table 4* it can be seen that, within experimental error, the agreement is quite good for networks prepared with $M_n = 1200$ at 0.0, 14.9, 30.0 and 48.9 wt% solvent and with $M_n = 2100$ in the bulk. The phantom network model underestimates the moduli for the networks prepared from $M_n = 1200$ at 69.9 wt% solvent and from $M_n = 2100$ at 20.4, 39.7, 50.0 and 59.9 wt% solvent. Affine and phantom networks are the extreme cases (above). The elastic behaviour of real networks obtained from stress–strain measurements falls between these limits. Previous studies[11] on telechelic POE have shown that the networks seem to have phantom chain behaviour when prepared with low-molecular-weight prepolymer and with high-molecular-weight prepolymer crosslinked at high dilution, results that are similar to those found here.

At the present level of discussion, the elastic free energy is given generally by:

$$\Delta A_{el} = C_1(\lambda_1^2 + \lambda_2^2 + \lambda_3^2 - 3) \qquad (14)$$

where λ_1, λ_2 and λ_3 are principal extension ratios. If $C_1 = \xi kT/2$, where ξ is the cycle rank, equation (14) is the change in the elastic free energy of a Gaussian phantom network[35]. In the theory under development in this laboratory, $C_1 = \mu kT\kappa_1 L_0^2/8\langle r^2\rangle_0$. Here μ is the number of junctions in the network, $L_0 = V_0^{1/3}$ is the length of the sample in the reference state, $\langle r^2\rangle_0$ is the mean-squared end-to-end distance of the chains connecting junctions, and κ_1 is the non-zero smallest eigenvalue of the Kirchhoff matrix, which has recently been shown[47] to be proportional to $\mu^{-2/3}$. We hope to analyse this system by means of calculations of κ_1 on very large systems at a future date to see if the network distribution theory offers an advantage over the cycle rank in predicting the modulus. Trends in the data[47] obtained to date suggest that it will. It is clear that the experimental reduced moduli for the tetrol–HDI systems studied here lie between the phantom and affine limits in all cases. We see no need to include an increment to the modulus from entanglements.

ACKNOWLEDGEMENTS

The authors are grateful for support for the Development of Energy, Grant DE-FG06-84ER45123. We also thank Professor R. F. T. Stepto for making his data available for use. This work is a contribution to an IUPAC-sponsored programme on the structure of polymer networks.

REFERENCES

1 Flory, P. J. 'Principles of Polymer Chemistry', Cornell University Press, Ithaca, NY, 1953
2 Stockmayer, W. H. *J. Chem. Phys.* 1943, **11**, 45; 1944, **12**, 125
3 Gordon, M. *Proc. R. Soc. Lond.* (*A*) 1962, **268**, 240
4 Macosko, C. W. and Miller, D. R. *Macromolecules* 1976, **9**, 199, 206
5 Dušek, K. and Vojta, V. *Br. Polym. J.* 1977, **9**, 164
6 Dušek, K., Gordon, M. and Ross-Murphy, S. B. *Macromolecules* 1978, **11**, 236
7 Stanford, J. L. and Stepto, R. F. T. *Br. Polym. J.* 1977, **9**, 124
8 Leung, Y. K. and Eichinger, B. E. *J. Chem. Phys.* 1984, **80**, 3877, 3885
9 Shy, L. Y., Leung, Y. K. and Eichinger, B. E. *Macromolecules* 1985, **18**, 983
10 Neuberger, N. A. and Eichinger, B. E. *J. Chem. Phys.* 1985, **83**, 884
11 Lee, K.-J. and Eichinger, B. E. *Macromolecules* (in press)
12 Shy, L. Y. and Eichinger, B. E. *Br. Polym. J.* 1985, **17**, 200
13 Shy, L. Y. and Eichinger, B. E. *Macromolecules* 1986, **19**, 2787
14 Galiatsatos, V. and Eichinger, B. E. *J. Polym. Sci., Polym. Phys. Edn.* 1988, **26**, 595
15 Hill, J. L. and Stepto, R. F. T. *Trans. Faraday Soc.* 1971, **67**, 3202
16 Yoon, D. Y. and Flory, P. J. *J. Chem. Phys.* 1974, **61**, 5366
17 Flory, P. J. and Chang, V. W. C. *Macromolecules* 1976, **9**, 33
18 Mark, J. E. and Curro, J. G. *J. Chem. Phys.* 1983, **79**, 5705
19 Mark, J. E., DeBolt, L. C. and Curro, J. G. *Macromolecules* 1986, **19**, 491
20 DeBolt, L. C. and Mark, J. E. *Macromolecules* 1987, **20**, 2369
21 Flory, P. J. 'Statistical Mechanics of Chain Molecules', Interscience, New York, 1969
22 Ilavský, M. and Dušek, K. *Polym. Bull.* (*Berlin*) 1982, **8**, 359
23 Ilavský, M. and Dušek, K. *Polymer* 1983, **24**, 981
24 Ilavský, M. and Dušek, K. *Macromolecules* 1986, **19**, 2139
25 Fasina, A. B. and Stepto, R. F. T. *Makromol. Chem.* 1981, **182**, 2479
26 Stanford, J. L. and Stepto, R. F. T. in 'Elastomers and Rubber Elasticity' (Eds. J. E. Mark and J. Lal), ACS Symp. Ser. 193, American Chemical Society, Washington, DC, 1982, Ch. 20
27 Stepto, R. F. T. in 'Biological and Synthetic Polymer Networks' (Ed. O. Kramer), Elsevier Applied Science, London, 1988, Ch. 10
28 Stepto, R. F. T. *Acta Polym.* 1988, **39**, 61
29 Stepto, R. F. T., private communication
30 Abe, A., Hirano, T. and Tsuruta, T. *Macromolecules* 1979, **12**, 1092
31 Abe, A. and Mark, J. E. *J. Am. Chem. Soc.* 1976, **98**, 6468
32 Saiz, E., Riande, E., Guzmán, J. and de Abajo, J. *J. Chem. Phys.* 1980, **73**, 958
33 International Mathematical and Statistical Libraries Inc. (IMSL), Program GGSPH
34 Nijenhuis, A. and Wilf, H. S. 'Combinatorial Algorithms', Academic Press, New York, 1975, Ch. 18
35 Flory, P. J. *Proc. R. Soc. Lond.* (*A*) 1976, **351**, 351
36 Abe, A., private communication
37 Abe, A., Hirano, T., Tsuji, K. and Tsuruta, T. *Macromolecules* 1979, **12**, 1100
38 Hoshen, J. and Kopelman, R. *Phys. Rev.* (*B*) 1976, **14**, 3438
39 Yan, J. F. *Anal. Chem.* 1965, **37**, 1588
40 Ahmad, Z. and Stepto, R. F. T. *Colloid Polym. Sci.* 1980, **258**, 663
41 Stepto, R. F. T. and Waywell, D. R. *Makromol. Chem.* 1972, **152**, 263
42 Treloar, L. R. G. 'The Physics of Rubber Elasticity', Clarendon, Oxford, 1975
43 Scanlan, J. *J. Polym. Sci.* 1960, **43**, 501
44 Case, L. C. *J. Polym. Sci.* 1960, **45**, 397
45 Pearson, D. S. and Graessley, W. W. *Macromolecules* 1978, **11**, 528
46 Flory, P. J. *Macromolecules* 1982, **15**, 99
47 Shy, L. Y. and Eichinger, B. E. submitted